Torsional Balance Thrust Measurement Techniques for Small RF Thrusters

Christopher M. Cretel*, Mazzin M. Ajamia†, Derek S. Thompson‡, and M. Umair Siddiqui§
Phase Four, Inc., El Segundo, CA, 90245, USA

A torsional, counter-balance thrust stand was developed to measure thrust over a range of 0.25 mN to 12 mN supporting the rapid iterative qualification of a 500 W electrodeless RF plasma thruster. This paper describes the design choices that mitigate the leading causes of error when measuring thrust on small RF thrusters. The design demonstrates improved immunity to RF interference, minimizes drift, and maintains detailed thruster telemetry, while supplying high resolution thrust measurements. Measurements of Phase Four's RFT are presented as an example of detailed uncertainty analysis and a description of best practices.

I. Nomenclature

A_{eff}	effective area of the calibration surfaces [m^2]
c	angular damping coefficient [N m s rad^{-1}]
C	correlation constant in electrostatic calibration [N m^2 V^{-2}]
D	calibration surface separation [μm]
F_{cal}	applied calibration force [mN]
F_t	thrust force [mN]
I	thrust stand moment of inertia [kg m^2]
L_{ODS}	moment arm of the optical displacement sensor [m]
L_t	moment arm of the thruster [m]
k_θ	angular spring constant [N m rad^{-1}]
k_{ODS}	linear spring constant from optical displacement sensor calibration [μN μm^{-1}]
V	applied voltage [V]
x_{ss}	steady-state linear position [μm]
X, Y, Z	Cartesian coordinates
Δx	position change measured by the optical displacement sensor [μm]
ζ	damping coefficient [dimensionless]
θ	angular position [radians]
θ_{ss}	steady-state angular position [radians]
ω_d	damped oscillation frequency [s^{-1}]
ω_n	un-damped natural frequency [s^{-1}]

II. Introduction

PHASE Four is developing a radio frequency (RF), electrodeless plasma thruster [1]. Electrodeless plasma sources are attractive for thruster applications because of their lack of hollow cathodes, a component of many legacy electric

*Propulsion Engineer, Phase Four, Inc., chris@phasefour.io
†Electrical Ground Systems Engineer, Phase Four, Inc. mazzin.ajamia@phasefour.io
‡Plasma Physicist, Phase Four, Inc., derek.thompson@phasefour.io
§Chief Technology Officer Intern, Phase Four, Inc., umair@phasefour.io

propulsion systems which restricts propellant choice, limits mission lifetime, and drives complex power electronics, costly manufacturing and restricted supply chains [2]. As RF thrusters (RFTs) emerge as a competing technology to the current industry standard of Hall effect thrusters and gridded ion engines, the development of accurate performance measurement techniques suitable for radio-frequency environments is paramount.

Several pendulum-type thrust balances have been developed for thrust measurements in the μN range [3–5] and others have been produced for larger systems [6, 7]. Phase Four has developed a torsional pendulum thrust balance to measure thrust between 0.25 mN and 12 mN with an uncertainty better than 10% of the measured thrust throughout that range. The most significant challenges associated with measuring thrust in the RFT are the electromagnetic and thermal environments the thruster generates during operation. The plasma in the vacuum chamber generates space charge around all surfaces, including the thrust stand, which produces parasitic electrostatic forces to the transducer. Changes in temperature of thrust stand feed-throughs cause harnessing to expand, contract, stiffen or loosen, displacing the thrust stand and affecting the spring constant. Finally, the RF environment transfers energy to sensors, generating time dependent "noise" and time averaged DC voltage offsets.

The RF signals generated by RFTs that must be accounted for to minimize electromagnetic interference are significantly different than those generated by Hall effect thrusters, gridded ion engines, and other DC plasma thrusters [8]. The Phase Four RFT technology operates near 10 MHz, significantly lower frequency than other"electron cyclotron resonance" style thrusters whose driving frequencies are in the GHz range [9]. In typical RF plasmas used for thrusters, plasma processing applications [10], RF heating and current drive for fusion applications [11], or laboratory apparatus [12], higher harmonics of the driving frequency are observed, with amplitudes typically more than 20 dB lower than the driving frequency. Furthermore, the plasma will have characteristic oscillations as a function of the local plasma density, average particle energy, magnetic field strength, and inter-particle collision frequency. Under certain conditions, signals will be generated at frequencies that represent sums and differences of other prominent signals in the plasma (through the action of "parametric instabilities" [13]). In sum, the electromagnetic spectrum that must be successfully filtered consists of the driving RF frequency, several harmonics, and other discrete and broadband regions of electromagnetic energy, modulated by the plasma system. To date, MIL-STD-461 radiated emission measurements have not been performed on an HF band electrodeless RF thruster.

This paper describes the processes developed to perform high fidelity thrust measurements on the Phase Four RFT. Section III sets the theoretical context for thrust measurements from pendulum dynamics. Section VI describes the development and fabrication of the torsional thrust balance and the steps taken to include RF power, telemetry, and propellant feed to the thruster without affecting the spring constant. Section VII describes the *in situ* method used to calibrate the thrust stand. This section outlines the process of converting raw data into a meaningful thrust measurement. A representative high fidelity thrust measurement in Phase Four's test facility is provided in Section VIII and compared with measurements taken at two other reference test facilities. Finally, Section IX presents best practices for torsional thrust measurements of RFTs. The needs of accurate thrust measurements in RF environments are more stringent than for non-RF thrusters. Consequently, techniques used to measure thrust in RFTs constitute best practices for thrust measurements of all thruster types.

III. Thrust stand operation

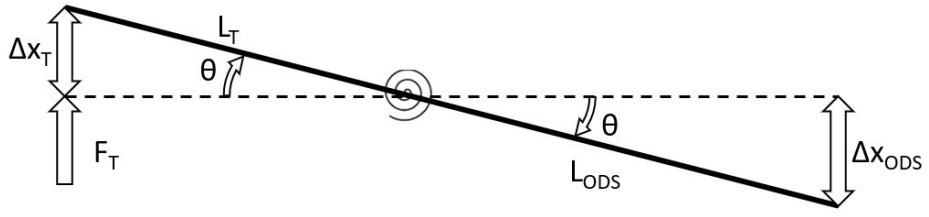

Fig. 1 Two dimensional diagram of the deflection of the thrust stand arm under an applied force at L

In torsional thrust balances, thrust is determined by measuring the displacement of a rotating arm. Reference [14] goes into great detail explaining the dynamics of thrust stands. A simplified, two-dimensional diagram is shown in Fig. 1. The spring constant is determined by applying a force, F_{cal}, and measuring a deflection at the displacement sensor, L_{ODS}.

Thrust is applied at a moment arm, L_T, while the deflection is still measured at the displacement sensor. The spring constant, k must be scaled by the mechanical advantage to account for the difference in moment arms, resulting in Eq. 1.

$$F_t = k\Delta x \frac{L_{\text{ODS}}}{L_t} \tag{1}$$

IV. The Phase Four VCH-1 test facility

RFT experiments were performed in Phase Four's large vacuum chamber, VCH-1 Dreadnought, shown in Fig. 2 and described in Ref. [1]. Dreadnought consists of a 152 cm diameter by 244 cm long cylindrical stainless-steel vacuum chamber. Five Shimadzu EI-V04M turbomolecular pumps pump at 10500 L/s for N_2. The turbomolecular pumps are backed by an Edwards iQDP80 dry rotary pump and iQMB1200 Roots pump stack. Above 10 Torr, the chamber pressure is monitored using an InstruTech convection gauge. At lower pressures, chamber conditions are monitored using an InstruTech ion gauge. Chamber base pressure is 10^{-6} Torr after approximately 48 hours of pumping. Background pressure during plasma production was $1.8 - 2.3 \times 10^{-5}$ Torr for mass flow rates between 3 and 10 sccm of xenon. A Stanford Research Systems (SRS) residual gas analyzer (RGA), calibrated to N_2 and mounted to the chamber wall, records the concentrations of gas and ion species in the chamber.

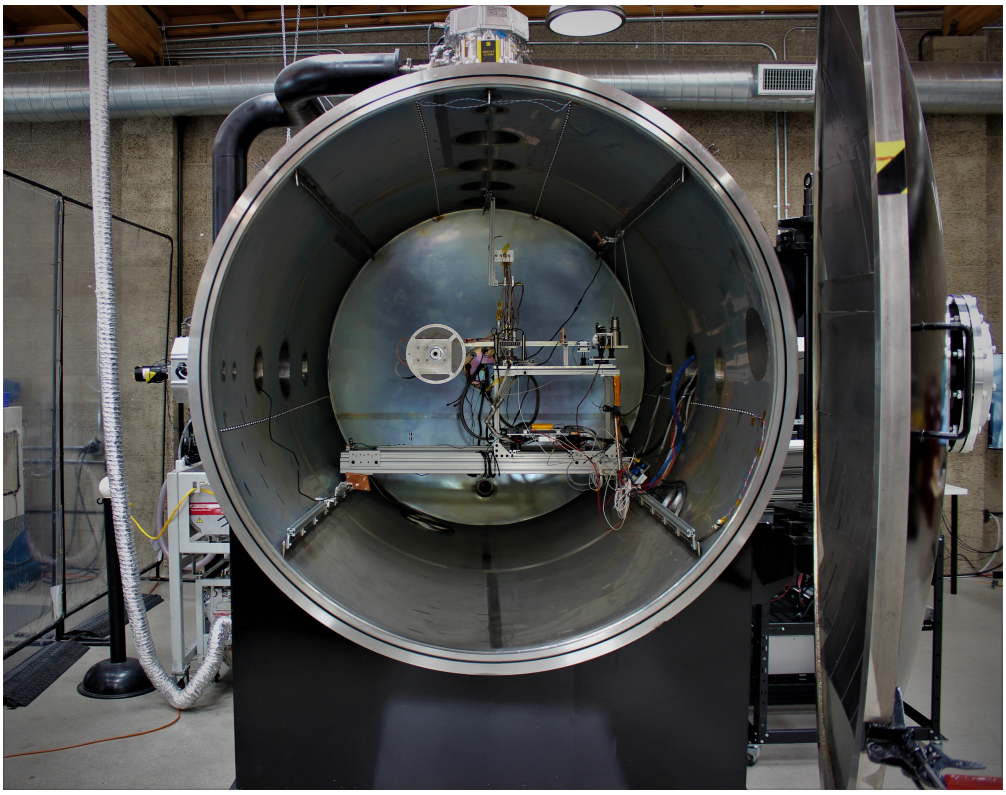

Fig. 2 Thrust stand experiments take place within the VCH-1 "Dreadnought" facility.

A thruster control unit (TCU) provides a comprehensive, portable controller and mock-flight computer. A PC-controlled SRS DS345 function generator sets the frequency and amplitude of a 1 kW custom Ophir RF amplifier. The resulting RF power is delivered to the thruster antenna via a 50 Ω RF coax using SMA and N-type connectors through a vacuum flange. Propellant feeds to the thruster through an MKS GM50A mass flow controller. Telemetry from the thruster is recorded by the PC using LabVIEW and a National Instruments cDAQ with at least 5 Hz sampling.

V. Performance metrics

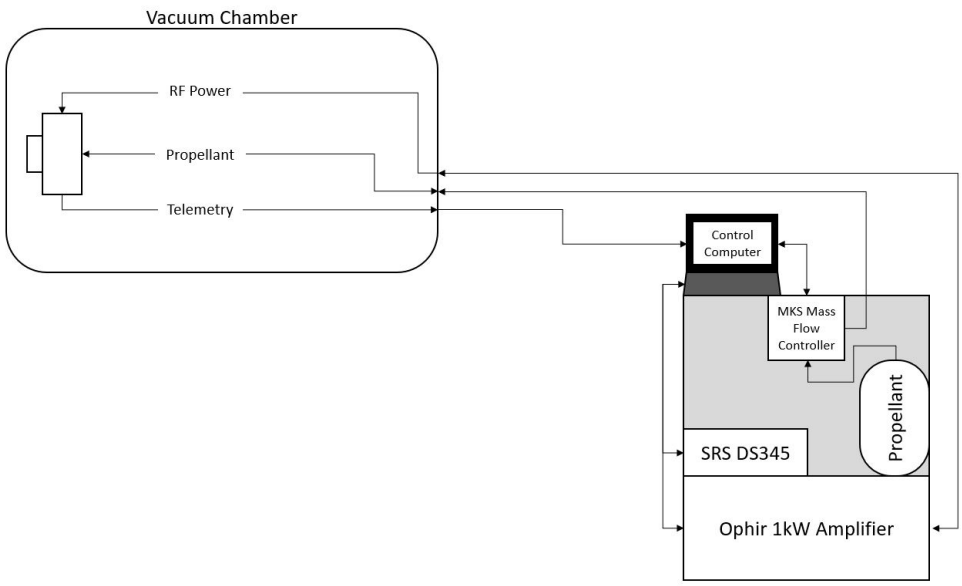

Fig. 3 A line diagram showing the main components of the RFT control and test setup.

Thrust stands are evaluated on a standard set of performance metrics [**?**]. Three are essential for successful thrust measurements: sensitivity, repeatability, and accuracy.

A. Sensitivity

Thrust stand sensitivity – the amount of deflection of the thruster stand arm from an applied force – sets the precision and resolution of thrust measurements. Eq. (1) indicates that small forces are best measured by maximizing the thrust stand arm lengths and minimizing the spring constant. Once the thrust stand arm length and spring constant are determined, sensitivity is set by the resolution and range of the sensor used for measuring displacement. Sensor selection is therefore a critical design choice.

B. Repeatability

Repeatability describes continued measurement confidence over an extended time. Measurements drift due to mechanical vibrations, thermal expansion, and angular variability in the spring constant. To control the linearity of the spring constant, any thrust stand interactions with cables and gas feeds should be minimized. As a general principle, error is reduced by placing cables and fuel lines as close to the pivot of the thrust stand as possible, minimizing the moment arm of unintended torque from these components. Smaller, flexible cables and gas feeds reduce the magnitude of unintended torque.

C. Accuracy

Along with developing an adequately sensitive and repeatable thrust stand, ensuring that the measurement is as near to the true value of the thrust is critical. Calibration methods should be tailored to best represent the environment under which the thrust stand experiences a force during operation. Each method should encompass the full range of thrust that is expected during the test campaign and should avoid any interference with thrust measurements when not being used.

To establish the accuracy of the thrust stand, the measurement is first calibrated to a known force before and a test campaign. The calibration is reconfirmed periodically throughout the campaign to minimize compounding error from measurement drift. The Phase Four thrust stand is calibrated in three ways. The first and primary method of calibrating

the spring constant is by using an electrostatic force that mimics a thrust response. Second, thrust stand consistency is checked by measuring the thrust from a known mass flow rate of a pure gas. These two methods are available while the chamber is at high vacuum. At atmosphere, a coarse check on these methods is conducted using a mass hanging over a pulley, in which gravity serves as the stand-in force.

VI. The Phase Four thrust stand

A schematic of the Phase Four torsional thrust stand is shown in Fig. 4. In its simplest form, the thrust stand consists of an arm that rotates about a flex pivot placed at the center of its length. The thruster is mounted at one end of the arm; counterweights and an optical displacement sensor (ODS) are placed at the opposite end. Eq. (1) provides calibrated thrust from the spring constant and the displacement reported by the ODS.

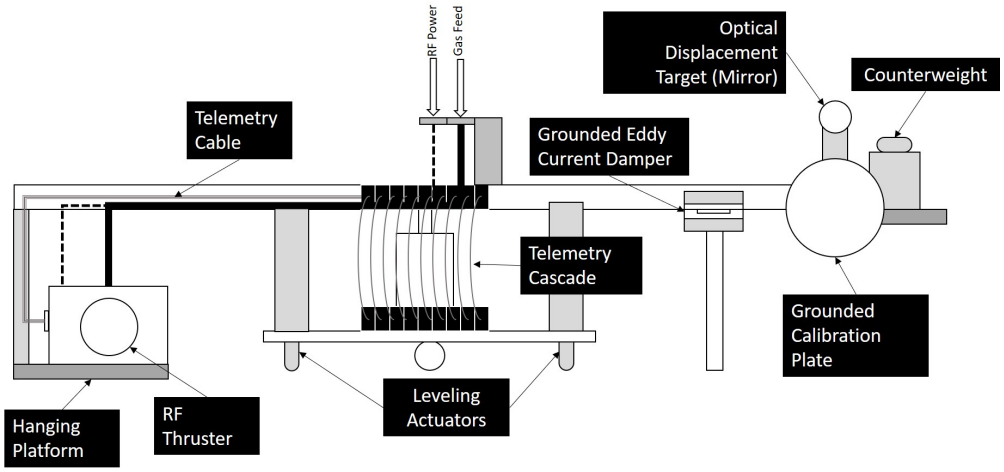

Fig. 4 Schematic of the Phase Four torsional pendulum thrust stand.

The thrust balance arm is a 2.5 cm × 7.6 cm × 91.4 cm hollow aluminum bar. This arm length improves thrust stand sensitivity by maximizing the thrust moment arm while keeping the thruster away from the chamber wall. Placing the point of rotation at the center of the balance arm minimizes the counterweight required to balance the thruster and decreases the load on the torsional spring. The torsional spring used is a Riverhawk 5016-400 cantilevered pivot bearing which has a nominal spring constant of 103.0 $\frac{mN-m}{\circ}$. For deflections of less than 13°, the estimated lifetime of the 5016-400 far exceeds the expected lifetime of the thrust stand, and hysteresis is minimal.

Aluminum platforms for the thruster and counterweights sit at opposite ends of the arm. The thruster platform hangs 15.2 cm below the thrust balance arm. The mass of the thruster stabilizes twisting along the length of the arm that leads to high frequency and amplitude noise in thrust signals. Rotational oscillations are damped with an eddy current damper, shown in Fig. 5. Eddy current dampers dissipate energy without introducing contact friction [7]. A copper bar mounted to the thrust stand passes between two strong, permanent magnets that are fixed 0.6 cm apart. Eddy currents induced by the motion of the copper in the magnetic field oppose thrust stand rotation. The damper is electrically grounded to the optical board to ensure that charge does not accumulate. Ungrounded damper charging in the plasma environment causes an erroneous reduction in measured thrust.

The thrust stand is mounted on a stainless steel base plate. Level control ensures that the base plate and thrust balance arm are aligned through the flex pivot. Two Newport TRA25CC actuators are mounted to adjacent corners of the base plate. A 1.9 cm stainless steel ball bearing is mounted in the middle of the opposite side, forming a tripod mount with the actuators. The actuators level the base plate according to a mounted circular bubble level. Counterweights are placed so that linear bubble levels mounted perpendicular to each other on the arm indicate that the arm is level.

Displacement is measured with a Philtec muDMS-RC32 ODS which reports the distance to a polished stainless steel mirror by detecting the intensity of reflected light. The ODS electronics outside the chamber are isolated from RF noise through fiber-optic transmission. Linear variable differential transformers (LVDTs), a type of displacement sensor used

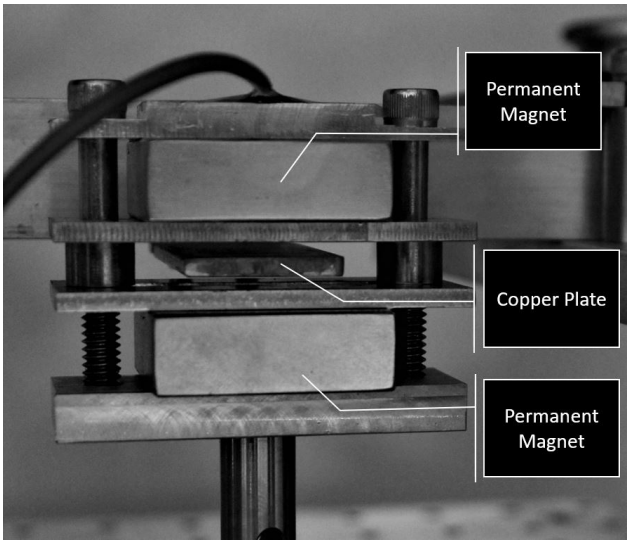

Fig. 5 An image of the eddy current damper used on the Phase Four torsional thrust stand.

on many thrust measurement apparatus, are not an option for the RFT because LVDTs are highly susceptible to RF noise and plasma interaction [15]. The ODS does not account for refraction in back surface mirrors, which are avoided.

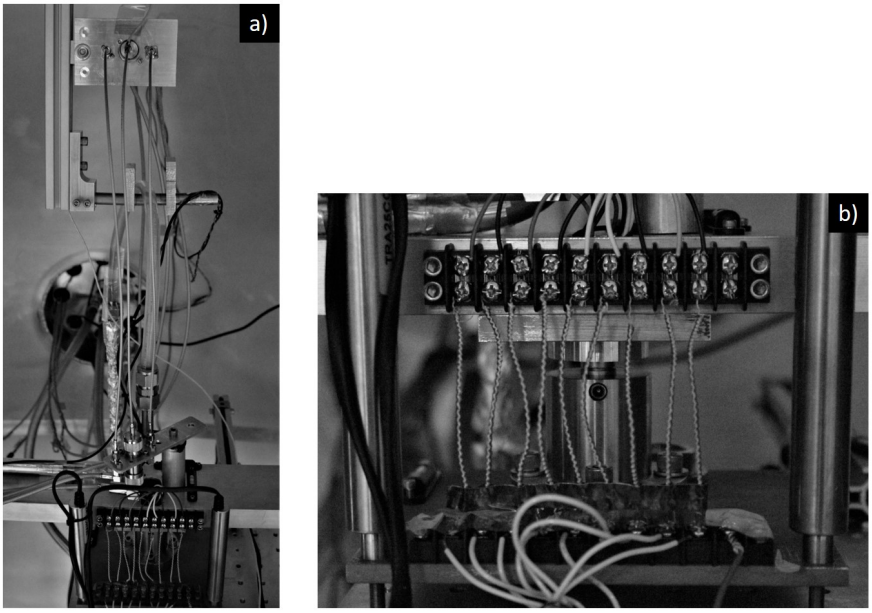

Fig. 6 a) RF power and power telemetry connected at the center of the thrust stand and b) thruster telemetry cascade.

Propellant is fed to the thruster through a 1/2 inch stainless steel tube. RF power transmits via RG400 coax cables fixed to the thrust stand arm with p-clamps. RF power runs along the length of the thrust balance arm to an RF power coupler which rests on the thruster platform. From the coupler, two RG400 cables return power measurements to the data acquisition software and the other supplies power to the thruster. Thruster telemetry, such as temperature, is passed through a nine-conductor cable in the hollow part of the thrust balance arm. Telemetry signals are transferred from the side of the thrust balance arm to the base plate at a screw terminal block using flexible 22 AWG wire.

All wiring and gas feed lines are mounted as close as possible to the pivot and directed normal to the thrust vector to minimize their effect on the spring constant [6]. The propellant feed enters the thrust balance vertically through flexible

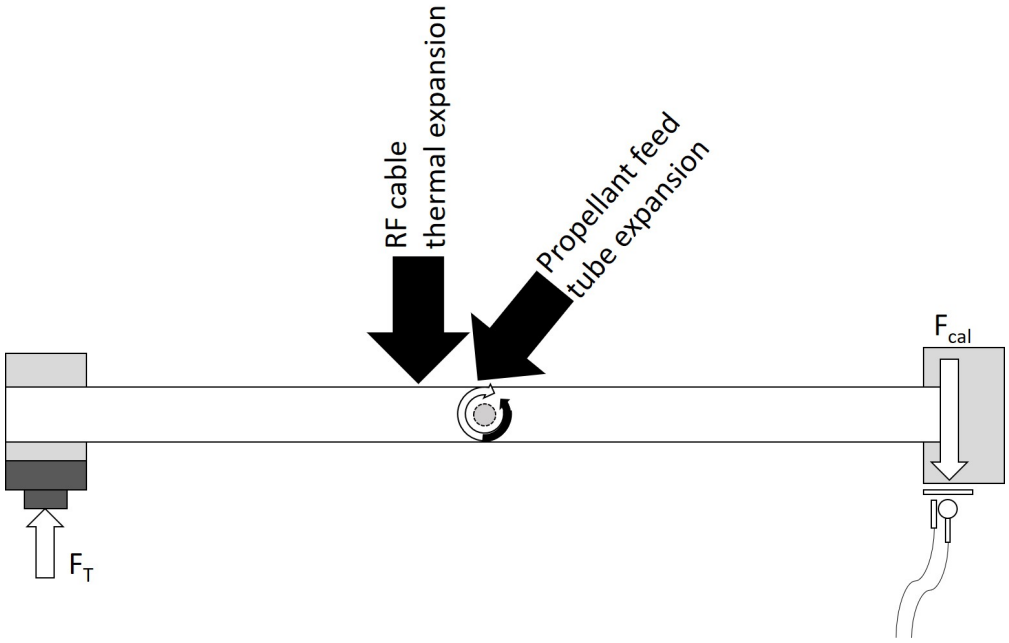

Fig. 7 Thermal expansion and expansion due to pressurized, flexible tubing appear as erroneous thrust and must be removed.

plastic tubing looped above the thrust stand, enabling the flexible tube to bend instead of twist. The three RF cables connect at the center to RG316 cables that run to a bulkhead above the thrust stand. These cables connect at a loose 90° angle to encourage bending instead of twisting of the cables.

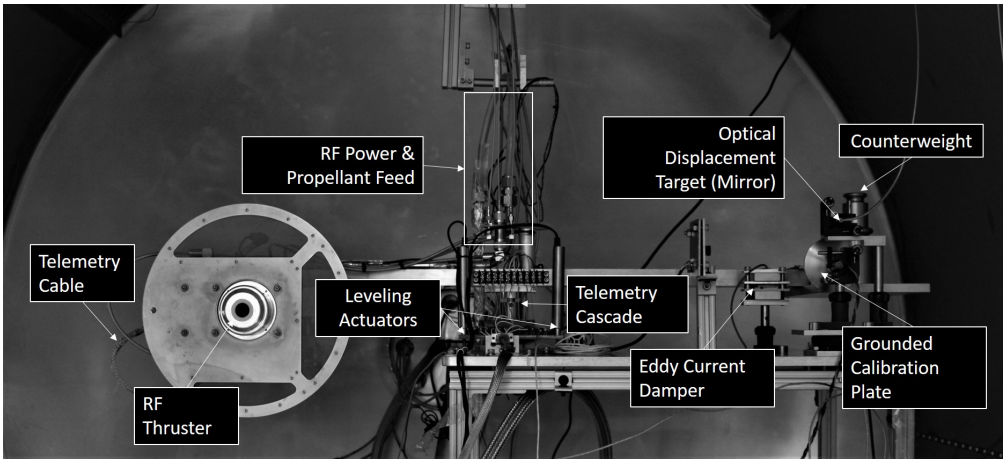

Fig. 8 Schematic of the Phase Four torsional thrust balance.

VII. Thrust stand calibration and analysis

A. Calibration force characterization and thrust stand calibration

The spring constant must be thoroughly characterized to obtain accurate thrust measurements. In situ calibrations use electrostatic forces between two conductors, as shown in Fig. 9. To do this, a 5.1 cm diameter aluminum flat plate is mounted to the thrust stand. Electrostatic potential is established between the flat plate and a 1.9 cm diameter stainless steel sphere. The high voltage surface is mounted with the ODS on a platform that translates perpendicularly to the thrust balance arm. The platform is remotely controlled with a Thorlabs MT1-ZA translation stage for fine movements, but distances are measured with the ODS because of error caused by backlash in the motorized stage. This process can be done in vacuum, does not physically contact the thrust stand, and under ideal conditions applies a force from 0.1 mN to 7 mN. The equation for an electrostatic force, F_{cal}, between two surfaces with an applied voltage between them takes the form

$$F_{\text{cal}} = C\left(\frac{V}{D}\right)^2 \tag{2}$$

where V is the applied voltage, D is the distance between the two plates, and C is an empirically determined correlation constant. Eq. (2) is a variation of the electrostatic force acting on two parallel flat plates where one plate is effectively infinitely large compared with the other. Because a spherical surface does not follow the equation directly, C is substituted to account for the variation.

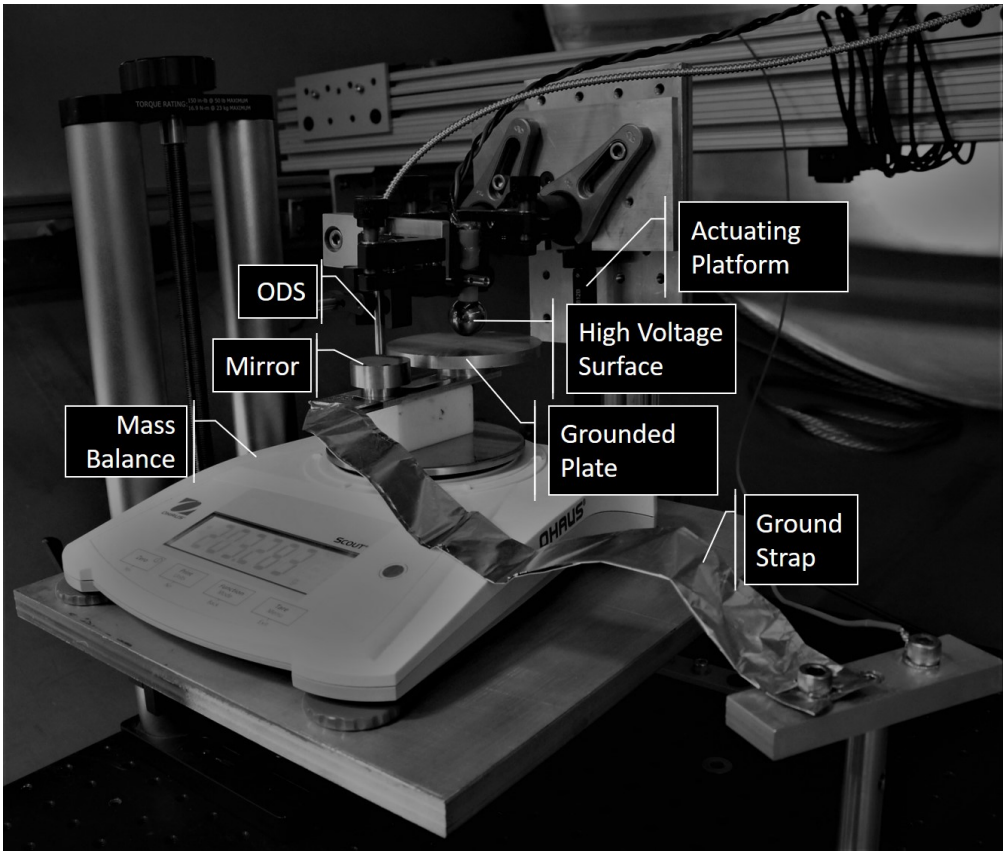

Fig. 9 Image of the electrostatic force calibration method arrangement.

In experiments comparing the spherical electrode to a flat-faced 1.3 cm diameter cylindrical electrode, the spherical configuration demonstrated several clear advantages. The spherical high voltage surface avoids electric field concentration at the edges of cylindrical electrodes. This improvement is especially pertinent when the two conductors are misaligned:

the spherical surface always presents the same radius regardless of alignment. Fig. 10 shows an exaggerated drawing of misaligned biased and grounded surfaces. Experimentally, the number of arcing events decreases when the spherical electrode is used. Arcing that does occur is observed at higher voltages and closer electrode separation compared with the cylindrical electrode. For a given potential and distance, the spherical configuration produces a smaller force. Fig. 11 shows sample characterization curves at 1000 µm and 1200 µm for voltages between 500 V and 4400 V applied to the sphere. C is observed to be dependent on electrode separation, which is accounted for during calibration.

The correlation constant is empirically characterized by measuring the lifting force applied at a given voltage and separation.The ground plate and ODS target rest on an OHauss Scout SPX mass balance while the high voltage surface and ODS are mounted on a vertically adjustable platform. The difference between the mass of the grounded plate and mirror assembly before and after the electrostatic force is applied determines the lifting force [3]. Between every data set, the apparatus is disassembled and rebuilt to account for variations in calibration assembly installation. The measurement is repeated several times for the each electrode separation to estimate the statistical spread. Fitting Eq. (2) to the voltage-force data for several separations produces C as a function of distance.

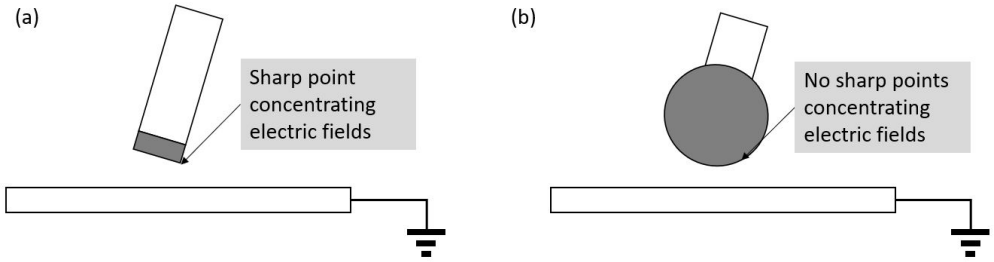

Fig. 10 a) Cylindrical parallel plate configuration that during severe misalignment; arcing occurs readily due to electric field concentrations at the edges of the cylinder face (b) the spherical configuration shows no variations despite electrode rotation.

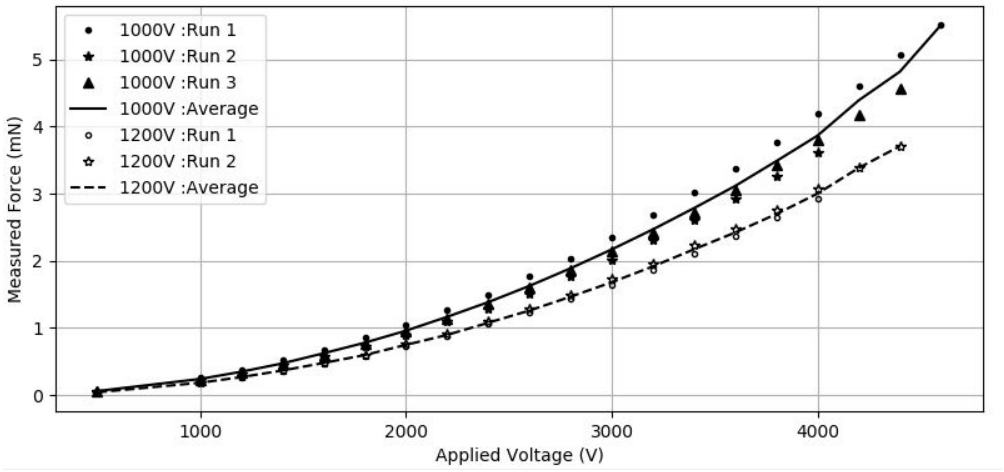

Fig. 11 Electrostatic force method calibration data using a biased sphere and a ground plate.

The thrust stand is calibrated with the thruster and all connections in place. Several points are chosen from a curve similar to the curve in Fig. 11 which span the full range of thrust expected for a given test campaign. To begin, an initial prediction of the spring constant is made based on previous results. The position of the high voltage surface is adjusted so that the thrust stand comes to rest at a well-characterized displacement after voltage is applied. High voltage is then applied. Once the thrust stand oscillations settle, the high voltage is shut off, allowing the thrust stand to return to its neutral position. The difference between the equilibrium displacement when force is applied and the neutral position after the force is shut off is used to update the spring constant.

$$k_{\text{ODS}} = \frac{F_{cal}}{\Delta x} \tag{3}$$

Note that Eq. (3) does not include a correction for moment arms because the calibration force acts at the same point along the thrust stand arm as the measurement is taking place. Once the linear spring constant k_{ODS} is determined, thruster force can be calculated using the relation from Eq. 1.

B. Corroborating spring constant characterization methods

The spring constant obtained by the electrostatic method is corroborated using masses hanging from the thrust stand over a polished stainless steel rod that act as a pulley. Weights are applied on the opposite side of the thrust balance arm from the electrostatic force plate, with equivalent moment arms. The weights and electrostatic forces rotate the arm in the opposing directions. Friction between the pulley and hanging wire disproportionately affects small weights, decreasing effective force acting on the thrust stand. The nylon thread used to connect the weight was slightly rigid, which also acted to decrease the effective force. The result was that the hanging mass method could only corroborate the spring constant at sufficiently large masses and suffered from large uncertainties.

Three masses are used, corresponding to 1.62 mN, 2.86 mN, and 6.08 mN. The thrust stand is allowed to settle after each weight is attached. The results are shown in Fig. 12. The hanging mass method had much more scatter than the electrostatic method but the two methods agreed within approximately 5 μN/μm.

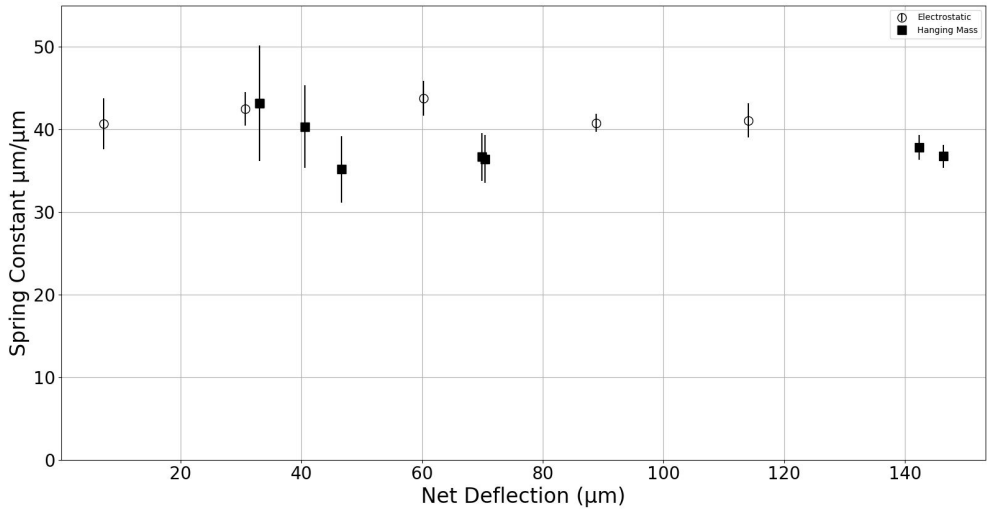

Fig. 12 The electrostatic calibration method compared to the hanging mass method.

C. Analysis

When analyzing thrust stand data, data produced by the ODS is plotted and lightly smoothed. The position recorded by the ODS when the thruster is firing is designated x_i. The position when power to the thruster is shut off is x_f. The neutral position of the thruster, x_n, is defined as the position when no external forces, including cold gas forces, are acting on the thrust stand. The total steady-state deflection is $\Delta x = x_n - x_i$ which accounts for cold gas and plasma forces. Thrust is derived from the measured Δx and the calibrated spring constant according to Eq. (**??**). All quantities associated with the thruster powered on are measured at the end of the thrust test which is when effects such as thermal drifts and cable expansion resemble conditions when the thruster will transition from on-to-off. The position x_f is measured soon after the thruster is turned off, because effects on long timescales do not affect the deflection due to thrust in the short term.

VIII. Thruster Testing

A calibration following the electrostatic procedure is done at the start of each test period, following a venting cycle, or whenever the thrust stand has not been used for a prolonged time. The test campaign begins after a consistent spring constant is achieved. Fig. 13 shows the response of the thrust stand when a 2.17 mN electrostatic force is applied with a 44.5 cm moment arm. Electrostatic calibration forces are applied at the point where the ODS is taking the measurement, L_{ODS}. Since the thruster has a 36.8 cm moment arm (L_t), a correction factor equal to the ratio of L_{ODS}/L_t is applied in Eq. (1). In this scenario $L_{ODS}/L_t = 1.21$.

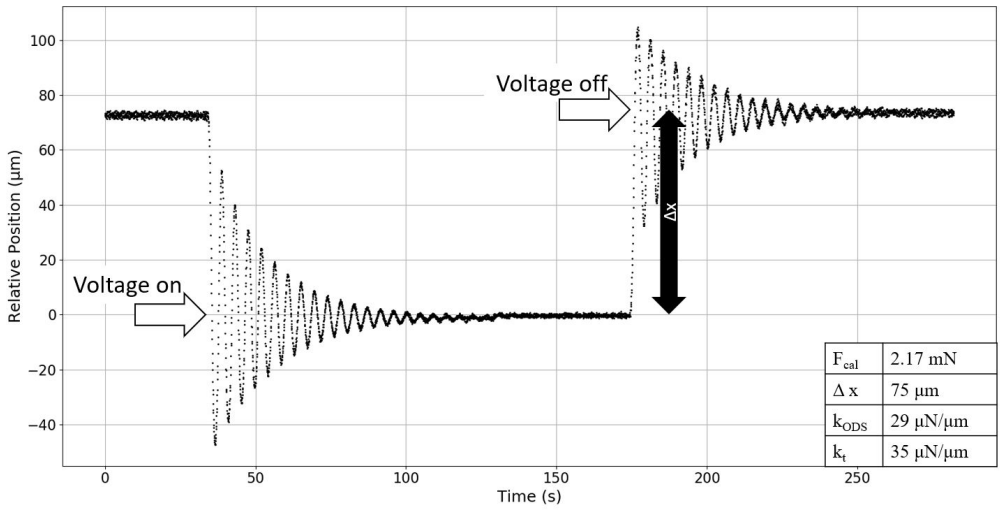

Fig. 13 A sampled electrostatic calibration applying 2.17 mN of force to characterize the spring constant of the thrust stand

In a typical thrust test, the thruster is ignited at a low power and a mass flow rate sufficient for ignition. After the thruster ignites, the mass flow rate is decreased to the desired test level. When the pressure in the chamber settles and the mass flow has reached a steady-state, power is increased to the test level. Once the thrust stand settles, power to the thruster is shut off. If a drift is present after shut-off, the deflection measurement is taken within the first three oscillations of the thrust stand so that the environment, including cable stiffness, cable thermal expansion, etc., are as similar to when the thruster was firing as possible. If there is no drift, the displacement can be recorded at anytime before the next firing.

Figs. 14 and 15 show examples of thrust stand measurements recorded with the Phase Four torsional thrust balance. The scales in these figures have been shifted such that the "zero" position is the point that the thruster achieves steady-state before being shut off. For reference, positive thrust rotates the thrust stand in a way that decreases the distance reported by the ODS.

A. Ignition with Xe

Fig. 14 shows thrust data while increasing RF power in a previously untested prototype thruster. At approximately 75 seconds, the mass flow controller begins flowing 30 SCCM of xenon. Between 150 seconds and 200 seconds, the thruster is ignited at 30 sccm but immediately extinguishes. After a successful second ignition attempt at 200 seconds, the mass flow rate is reduced to 10 sccm of xenon which presents itself as an increase in the distance reported by the ODS. Power is increased between 225 seconds and 250 seconds to the nominal power setting of 240 W into the thruster. As power increases, the thrust stand responds with a decrease in displacement, indicating that thrust increases with power. Once the desired power is achieved at ≈250 W, the thrust stand settles. The deflection is not expected to change, however a drift is observed. This drift is absent once power to the thruster is shut off, and the thrust stand returns to its original position.

The cause of the drift emerges by examining the thrust and RF power histories. While the thruster is supposedly operating at steady-state, forward power decreases over time. A rapid decrease in forward power corresponds to an

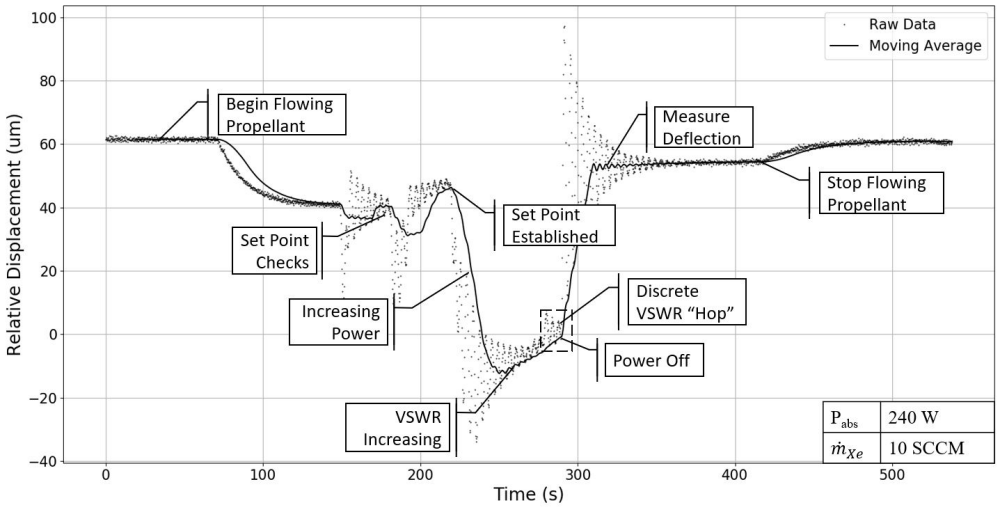

Fig. 14 RFT showing proper power termination response

amplitude change in the oscillations of the thrust stand at 275 seconds before shutting off a few seconds later. This behavior is a result of the voltage standing wave ratio (VSWR) of the thruster changing in response to changes in the plasma. VSWR is a measure of how well the impedance of an antenna is matched to its transmission line. Variations in VSWR occur when the RFT plasma responds to changes in mass flow rate or to contaminants entering the liner. It is observed that as the thruster temperature increases, water particles began to de-sorb from the liner, injecting impurities into the plasma and changing its electrical properties. In consequence, the VSWR degraded and thrust decreased. Stable thruster operation is achieved by prolonged operation to pre-heat the thruster and remove water from the liner before recording data for the research campaign.

As an alternative example, Fig. 15 shows the thrust stand response to decreasing the mass flow rate too soon after the thruster powers down. As in the previously described test, 30 sccm of xenon is used to ignite the thruster. A small displacement toward zero at 230 seconds indicates that the thruster ignited at a low power. The larger deflection away from zero immediately following is the mass flow rate decreasing to 10 sccm, the nominal flow rate for this test. Note that the deflection of the thrust stand is the same for the same flow rate as in Fig. 14 at 225 seconds. These results show the repeatability of the thrust stand, as these tests were done four months apart with only minor alterations to the thrust stand.

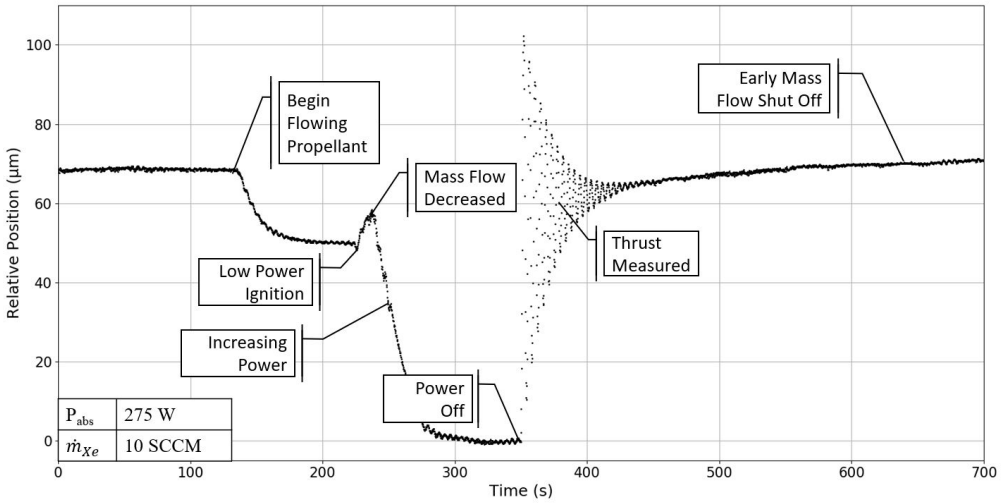

Fig. 15 Thrust stand data following early reduction in mass flow rate

Once the thruster is ignited, the power is gradually increased to 275 W, and allowed to equilibrate. At 350 seconds, power to the thruster was shut off and the thrust stand deflects accordingly. Some time between 350 seconds and 400 seconds, the mass flow rate was shut off prematurely. A decreasing mass flow rate introduces logarithmic behavior superimposed on the damped harmonic oscillator function of the thrust stand, as the propellant lines purge the remaining propellant. To avoid this behavior, mass flow is typically terminated well after the thrust stand has damped its oscillations to better isolate thrust stand response to the plasma. Fig. 14 demonstrates this clearly as the thrust stand is allowed to settle between 350 and 400 seconds and mass flow is shut off at about 415 seconds.

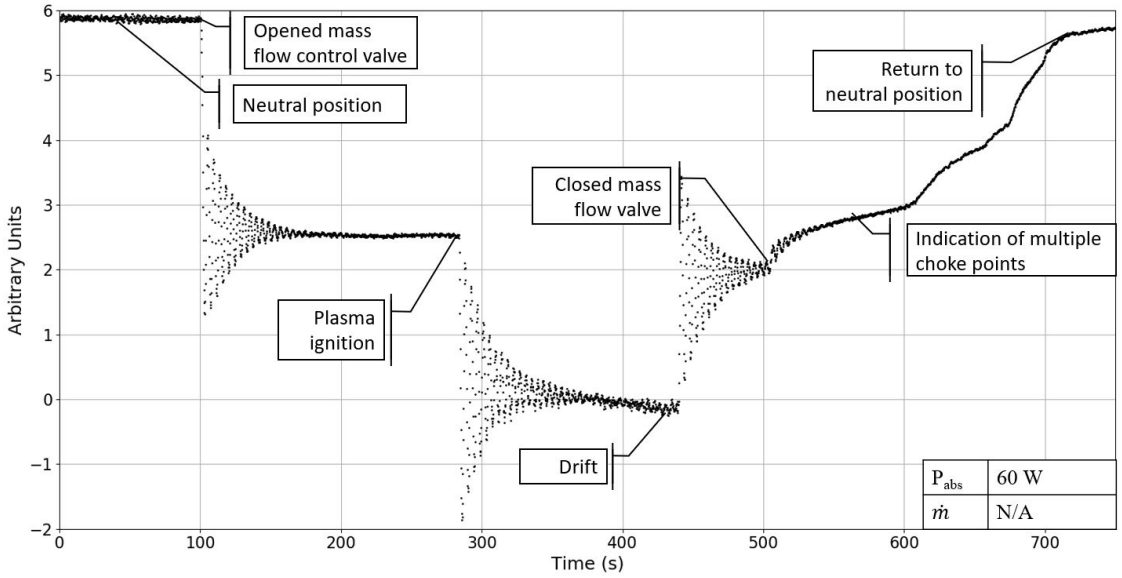

Fig. 16 Thrust stand data for an RFT firing using unconventional propellant with arbitrary units

Fig. 16 demonstrates the thrust stand's ability to flow on non-noble gas propellants. Impulsive behavior is observed by the thrust stand as the flow control valve is opened at 100 seconds. Allowing to setter for for nearly 2 minutes, the RFT ignites at 290 seconds and the thrust stand is again allowed to settle to a steady-state deflection. As with Fig. 14, a drift is observed, however this drift contributes positively to the measured thrust. Similarly, the drift is not observed when power to the thruster is shut off, suggesting that the thrust is increasing slightly over time. This drift is small compared to the total deflection of the thrust stand and is within the uncertainty of the measurement. The thrust stand was allowed to settle before shutting the mass flow control valve, however very strange behavior followed. Between 500 seconds and the end of the data set at 750 seconds, several structures resembling square roots are observed. This indicates that there are several locations in the propellant feed line that, for this propellant, cause choked flow as a function of the decreasing upstream pressure. This is a facility affect that does not seem to contribute to uncertainties while firing but will be addressed in the future.

The Phase Four RFT has been tested at three separate facilities. Fig. 17 plots the data from the three facilities as well as demonstrative data of *Maxwell*, Phase Four's first product. All of the data that is presented in Fig. 17 flows 10 sccm of xenon as the propellant. The RFT was tested at the Aerospace Corporation in El Segundo, CA at low powers around 50 W[**?**]. The thrust stand used there is a torsional pendulum type, a similar system is discussed in Ref. [3]. Tests at the undisclosed facility were done up to 250 W and on an inverted pendulum designed for higher power and heavier test articles. Tests at Phase Four have reached nearly 500 W. From 50 to over 250 W, Phase Four's torsional pendulum thrust balance correlates with both third party facility's thrust stands. Thrust measurements above 250 W were only done at Phase Four but follow linearly with the lower power data. Error bars are much larger that what will be presented under uncertainties because there was an uncommon amount of drift while firing that has since been resolved.

B. Uncertainties

Uncertainty analysis was undertaken to identify error in measured thrust. The most significant sources of systematic error are the ODS, the Ohauss Scout SPX223, and the high voltage power supply. The ODS always measures distances

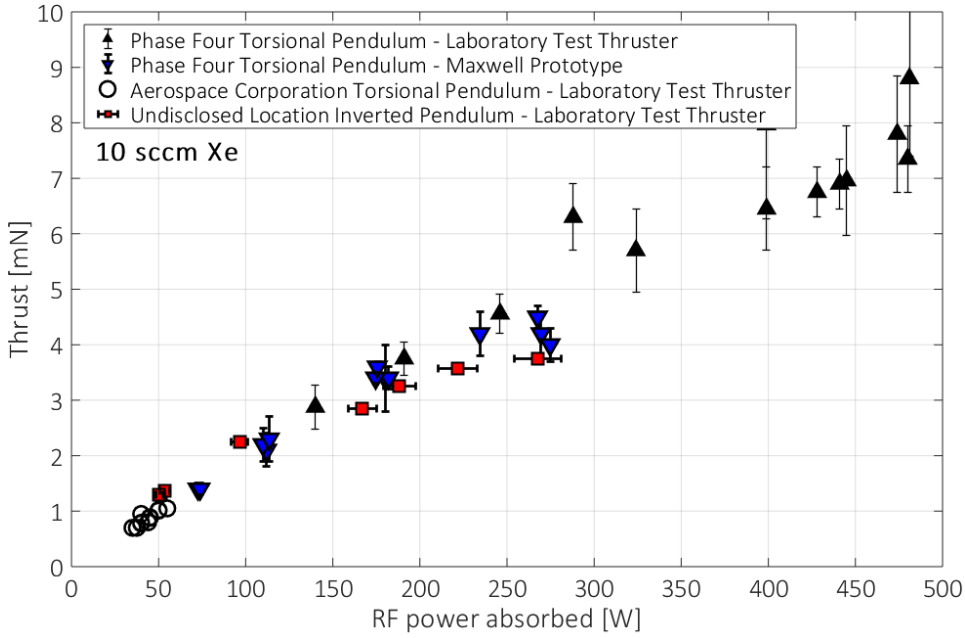

Fig. 17 Phase Four has tested a laboratory test thruster at two third-party facilities and show that data from each corroborates with the Phase Four torsional balance thrust stand

as they pertain to the thrust stand. The Ohauss measures the weight difference when characterizing the calibration surfaces, the high voltage power supply delivers the potential different across the calibration surfaces and the tape measure measures the moment arms of the ODS and thruster. All systematic uncertainties stem from these four devices. Other uncertainties are procedural. These include the stability of the mass flow rate and RF power (VSWR), and whether the duration of the fire allows for thermal drift. As shown in Tab. 1, the procedural uncertainties dominate the analysis.

Table 1 Table of contributions to thrust measurement uncertainty

Uncertainty Source	Uncertainty @ 0.25 mN	Uncertainty @ 20 mN
High voltage power supply resolution and accuracy	±0.004 mN	±0.010 mN
Optical displacement sensor accuracy	±0.002 mN	±0.007 mN
Effective area calculation	±0.060 mN	±0.600 mN
Measurement of the ODS moment arm	±0.010 mN	±0.100 mN
Measurement of the thruster moment arm	±0.014 mN	±0.140 mN
Measuring deflection from thrust	±0.070 mN	±0.700 mN
Total uncertainty	±0.080 mN	±1.000 mN

Measuring the deflection due to the thruster firing had the most significant contribution to the total uncertainty. This is due to transients that present themselves in the thruster itself and not in the thrust stand design. When a stable equilibrium cannot be achieved by the thruster, the estimates for measuring the deflection are $\leq$ 10% of the total deflection. The ability to read the absolute position from the ODS is usually within ±1 μm for a stably run thruster. The second most significant source of error comes from measuring the effective area of the round calibration surface which incorporates uncertainties in set up and mass measurements. Further development will improve this calculation.

IX. Conclusion

Phase Four has developed a torsional thrust stand that is optimized for high-resolution, repeatable, and accurate mN-scale thrust measurements in RF plasma environments. Error arises predominantly from the connections going to the thrust stand and from unstable thruster operational modes. Thermal expansion causes drifts during operation and low frequency vibrations show up as noise when a cable is not secured correctly. Both of these effects are eliminated when testing integrated thrusters for flight. Improved calibration techniques and noise insensitivity permit the characterization of thrusters at high RF power and with propellants beyond the noble gases while ensuring high confidence in measured thrust. The advances incorporated into the Phase Four thrust stand make it suitable for sensitive measurements in harsh RF environments, however the noise and error sources it is designed to mitigate broadly affect electric propulsion thrust measurements as a class. As such, these error mitigation strategies apply to any electric propulsion thrust measurement.

Acknowledgments

References

[1] Siddiqui, M. U., and Cretel, C., "Updated Performance measurements and Analysis of the Phase Four RF Thruster," *Joint Propulsion Conference*, AIAA, Cincinnati, OH, 2018.

[2] Khayms, V., and Martinez-Sanchez, M., "Design of a miniaturized Hall thruster for microsatellites," *AIAA, ASME, SAE, and ASEE Joint Propulsion Conference and Exhibit*, AIAA, Buena Vista, FL, 1996.

[3] Hsu, A., Beiting, E., and Curtiss, T., "Performance of a Torsional Thrust Stand with 1 μN Sensitivity," IEPC-2015-261.

[4] Lam, J., Koay, S., and Cheah, K., "Electromagnetic calibration system for sub-micronewton torsional thrust stand," 2017.

[5] Kobling, M., Monette, M., Weikert, M., and Tajmar, M., "The SpaceDrive Project - Thrust balance development and new measurements of the Mach-Effect and EMDrive Thrusters," *Acta Astronautica*, Vol. 161, 2019, pp. 139–152.

[6] Kunning, W. M. L., Xu G, "High-power,null-type, inverted pendulum thrust stand," *American Institute of Physics*, Vol. 80, 2009, pp. 80–86.

[7] Markusic, T., Jones, J., and Cox, M., "Thrust stand for electric propulsion performance evaluation," *Review of Scientific Instruments*, Vol. 77, No. 10, 2006. doi:10.1063/1.2357315.

[8] Beiting, E. J., Eapen, X. L., Pollard, J. E., Gambon, M., Marchandise, F. R., and Oberg, M., "Electromagnetic Emissions from PPS 1350 Hall Thruster," *International Electric Propulsion Conference*, IEPC, Ann Arbor, MI, 2009.

[9] Jarrige, J., Elias, P.-Q., Cannat, F., and Packan, D., "Performance Comparison of an ECR Plasma Thruster using Argon and Xenon as Propellant Gas," *International Electric Propulsion Conference*, IEPC, Washington, DC, 2013.

[10] Hopwood, J., "Review of inductively coupled plasmas for plasma processing," *Plasma Sources Science and Technology*, Vol. 1, No. 109, 1992.

[11] Cardinali, A., Castaldo, C., Cesario, R., Amicucci, L., Galli, A., Napoli, F., Panaccione, L., Riccardi, C., Santini, F., Schettini, G., and Tuccillo, A. A., "Radio-frequency current drive for thermonuclear fusion reactors," *Nature*, Vol. 8, No. 10318, 2018.

[12] Siddiqui, M. U., Thompson, D. S., Jackson, C. D., Kim, J. F., Hershkowitz, N., and Scime, E. E., "Models, assumptions, and experimental tests of flows near boundaries in magnetized plasmas," *Physics of Plasmas*, Vol. 23, No. 057101, 2016.

[13] Kline, J. L., and Scime, E. E., "Parametric decay instabilities in the HELIX helicon plasma source," *Physics of Plasmas*, Vol. 10, No. 1, 2003.

[14] Polk, J., and et al., "Recommended Practice for thrust measurement in electric propulsion testing," *Review of Scientific Instruments*, Vol. 33, No. 3, 2017. doi:10.2514/1.B35564.

[15] Ziemer, J., "Performance Measurements Using a Sub-Micronewton Resolution Thrust Stand," 2001.